INVITED PAPER

High-Temperature Tunneling Quantum-Dot Intersublevel Detectors for Mid-Infrared to Terahertz Frequencies

Devices with multiple layers of dots offer reduced dark current and promise future development of infrared photodetectors that operate at moderately low temperatures or even at room temperature.

By Pallab Bhattacharya, *Fellow IEEE*, Xiaohua Su, G. Ariyawansa, and A. G. U. Perera

ABSTRACT | Quantum-dot infrared photodetectors have emerged as attractive devices for sensing long wavelength radiation. Their principle of operation is based on absorption of radiation via intersublevel transitions in quantum dots. Multiple layers of self-organized In(Ga)As/Ga(Al)As quantum dots are generally incorporated in the active region of these devices. Three-dimensional quantum confinement allows normal incidence operation. This paper describes a novel variation in the design of these devices which allows a significant reduction of the dark current, high temperature operation and extension of operation to terahertz frequencies. The principle of operation and operating characteristics of this device—the tunnel quantum-dot intersublevel detector—are described. Operation is demonstrated from 6–80 μm at temperatures up to 300 K with acceptable values of peak responsivity (0.1–0.75 A/W) and specific detectivity (10^7–10^{11} cm $\cdot$ Hz$^{1/2}$/W^{-1}, depending on temperature and wavelength).

KEYWORDS | GaAs; InAs; infrared detector; quantum dots; responsivity; specific detectivity; terahertz detection

Manuscript received October 27, 2006; revised April 11, 2007. This work was supported in part by the Army Research Office and in part by the National Science Foundation.

P. Bhattacharya and **X. Su** are with the Solid State Electronics Laboratory, Department of Electrical Engineering and Computer Science, University of Michigan, Ann Arbor, MI 48109-2122 USA (e-mail: pkb@eecs.umich.edu).

G. Ariyawansa and **A. G. U. Perera** are with the Department of Physics and Astronomy, Georgia State University, Atlanta, GA 30303 USA.

Digital Object Identifier: 10.1109/JPROC.2007.900968

I. INTRODUCTION

A significant reduction in the cost of an infrared camera is possible if the traditional cooling systems with liquid nitrogen are replaced by thermoelectric coolers, or the array can be operated at room temperature. There is, therefore, an urgency to develop infrared photodetectors that operate at elevated temperatures. The quantum-dot infrared photodetector (QDIP) [1]–[3] has emerged as an interesting and potentially viable device, wherein three-dimensional quantum confinement promises low dark currents, leading to a large detectivity. Additionally, in these devices, polarization selection rules allow absorption of normally incident light and the long effective carrier lifetime ~hundreds of picoseconds, confirmed by theory [4] and experiment [5], provides the potential for large responsivity. Rapid progress has been made in the development of these devices and recently reported performance characteristics [6]–[12] (peak responsivity $\geq$ 0.5 A/W and specific detectivity $\sim 10^{10} - 10^{11}$ cm $\cdot$ Hz$^{1/2}$/W in the temperature range ~80–150 K) are cause for optimism.

Unlike that in bulk p-n junction detectors or in quantum-well infrared photodetectors (QWIPs), the density of states of the self-organized In(Ga)As/GaAs quantum dots in QDIPs is represented by broadened δ-functions for the electron and hole ground and excited states. Even though the density of states is discrete for low energy states, it tends to become like three-dimensional continuous states at high energies. As a result, at temperatures above ~150 K, the electron occupation is dominated by the excited states. Therefore, in the conventional QDIP,

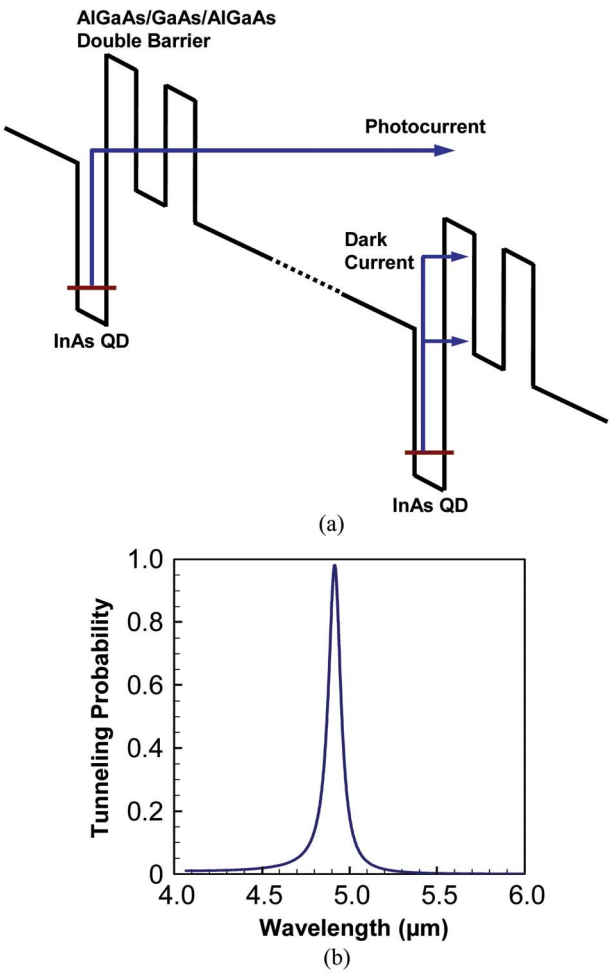

Fig. 1. *Schematic diagram of: (a) the conduction band profile of an InAs/GaAs T-QDIP, using resonant AlGaAs double-barriers, and (b) tunneling probability of double barrier as a function of wavelength, demonstrating a peak wavelength of 4.9 μm under a bias voltage of 1.2 V.*

dark current benefits are difficult to sustain at high temperatures. The reduction of dark current at high temperatures of operation is one of the biggest challenges in the design of QDIPs. The problem stems from the commonality of the transport paths of carriers contributing to the dark current and photocurrent. Hence, any heterostructure design aimed at reducing the dark current also reduces the photocurrent and responsivity.

In this paper, we describe the properties of a novel device—a tunneling QDIP (T-QDIP)—in which a resonant tunneling heterostructure is incorporated with each quantum-dot layer [13]–[16]. The conduction band diagram is schematically shown in Fig. 1(a). The resonant tunneling double barrier is so designed that the electron tunneling probability is unity at an energy coincident with the peak detection wavelength, as shown in Fig. 1(b). The tunneling probability will be significantly smaller at energies which are removed from this optimum value. Thus, the transport of the carriers contributing to the dark current, which have a broad energy distribution at high temperatures, will be inhibited and the dark current will be reduced. We show here that the T-QDIP can be a very versatile device for insertion in high temperature focal plane arrays (FPAs) suitable for several wavelength ranges of interest.

In what follows, suppression of dark current in T-QDIPs is demonstrated in Section II, both theoretically and experimentally. The characteristics of devices designed for midinfrared (MIR) and far-infrared (FIR) are presented in Section III. The detection of terahertz (THz) radiation with the T-QDIPs is described in Section IV. Conclusions are drawn in Section V.

II. DARK CURRENT SUPPRESSION IN T-QDIP

The dark current in a QDIP, as a function of applied bias V, is given by

$$I_D(V) = ev(V)n_{\mathrm{em}}(V)A \tag{1}$$

where v is the average electron drift velocity in the barrier material, n_{em} is the concentration of electrons excited out of the quantum dots by thermionic emission and tunneling, and A is the detector area. Here

$$v(V) = \frac{\mu F(V)}{\sqrt{1 + (\mu F(V)/v_s)^2}} \tag{2}$$

and

$$n_{\mathrm{em}}(V) = \int_{-\infty}^{\infty} N(E)f(E)T(E,V)dE \tag{3}$$

where μ is the electron mobility, F is the bias-dependent electric field, v_s is the electron saturation velocity, $f(E)$ is the Fermi–Dirac distribution function, $N(E)$ is the density of states, and $T(E,V)$ is the tunneling probability across a triangular barrier. Here E is the total energy, rather than the energy associated with the tunneling direction, since in a real system electron scattering causes the electron wave function to decay in the barriers in accordance with the total energy of the electrons. The tunneling probability is calculated using the transfer matrix method. For both square and triangular potential barriers, segmentation was employed to simplify the calculations, wherein the barrier potential is a constant V_j in the jth segment.

The corresponding one-dimensional plane wave associated with the electron is

$$\psi_j(z) = A_j \exp(ik_j z) + B_j \exp(-ik_j z) \tag{4}$$

where $k_j = 2\pi\sqrt{2m_j^*(E - V_j)}/h$, h is Planck's constant and m_j^* is the effective mass. The tunneling probability is then given by

$$T(E) = m_{N+1}^* k_0 / \left(m_0^* k_{N+1} M_{22}^2\right) \tag{5}$$

where M_{22} is the element of the transfer matrix $\prod_{n=1}^{N+1} M_n$ with both column and row index equal to 2. The subscripts 0 and $N+1$ correspond to points outside the barriers. The density of states $N(E)$ is given by

$$N(E) = \sum_i \frac{2N_d}{L_p} \frac{1}{\sqrt{2\pi}\sigma} \exp\left(\frac{(E - E_i)^2}{2\sigma^2}\right) + \frac{4\pi m^*}{L_p h^2} \times H(E - E_W) + \frac{8\pi\sqrt{2}}{h^3} m^{*3/2} \sqrt{E - E_C} H(E - E_C) \tag{6}$$

where, in the first term, N_d is the surface density of the dots and E_i is the energy of the discrete dot levels. The values of E_i are determined from an eight-band $\mathbf{k} \cdot \mathbf{p}$ calculation [17], [18], assuming a pyramidal shape of the dots and accounting for built-in strain through the valence force field model. A Gaussian distribution accounts for the inhomogeneous broadening due to size inhomogeneity of the dots. The second term is the density of the wetting layer states, which is calculated by assuming a two-dimensional electron gas in the wetting layer. E_w is the energy of the wetting layer state and since the thickness of the wetting layer is small (less than two monolayers), only one confined state exists in this layer. The function $H(x) = 1$ for $x \geq 0$ and $H(x) = 0$ for $x < 0$. The last term gives the density of states in the bulk barrier material and E_c is the energy of the conduction band edge therein.

Equations (1)–(6) are used to calculate the dark current in a conventional QDIP without tunnel barriers. The same equations can also be used to calculate the dark currents in a T-QDIP after suitable modification of the density of states $N(E)$ and the tunneling probability $T(E, V)$ for the double barrier resonant tunneling heterostructure. We have calculated the dark current density for two sets of conventional and tunneling QDIPs. The heterostructures for one set are schematically shown in Fig. 2(a) and (b). Nominally, the total thickness of each dot period is the same in the conventional and tunnel QDIPs, so that the electric field in the active region under the same bias is nearly identical in all four devices. The calculated dark current densities of the devices shown in Fig. 2 as a function of bias at 150 K and 200 K are shown in Fig. 3(a) and (b), respectively. A reduction in the dark current density by approximately two orders of magnitude is expected in the T-QDIP compared to the conventional design. The oscillation in the calculated TQDIP dark current density is due to quantum resonant tunneling. This oscillation has not been observed in real devices. The reason is that multiple resonant double barriers can smooth the oscillations in the dark current by scattering.

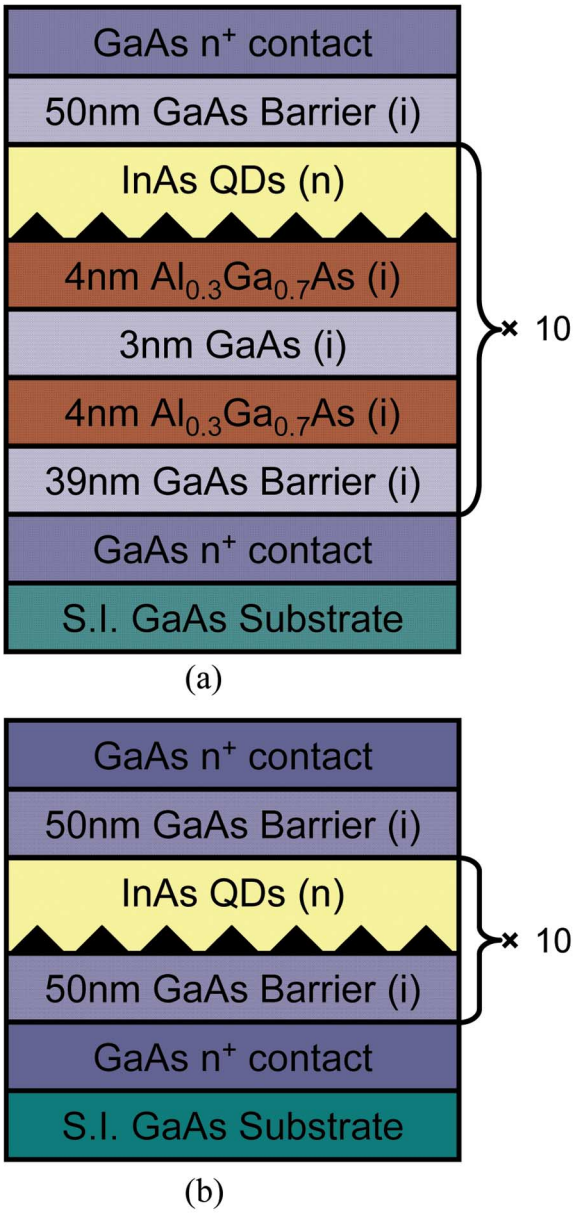

Fig. 2. *Schematics of heterostructures of: (a) tunnel QDIP and (b) conventional QDIP, grown by molecular beam epitaxy.*

The conventional and tunneling QDIP for MIR operation, with heterostructures shown in Fig. 2(a) and (b), respectively, were epitaxially grown and fabricated. The

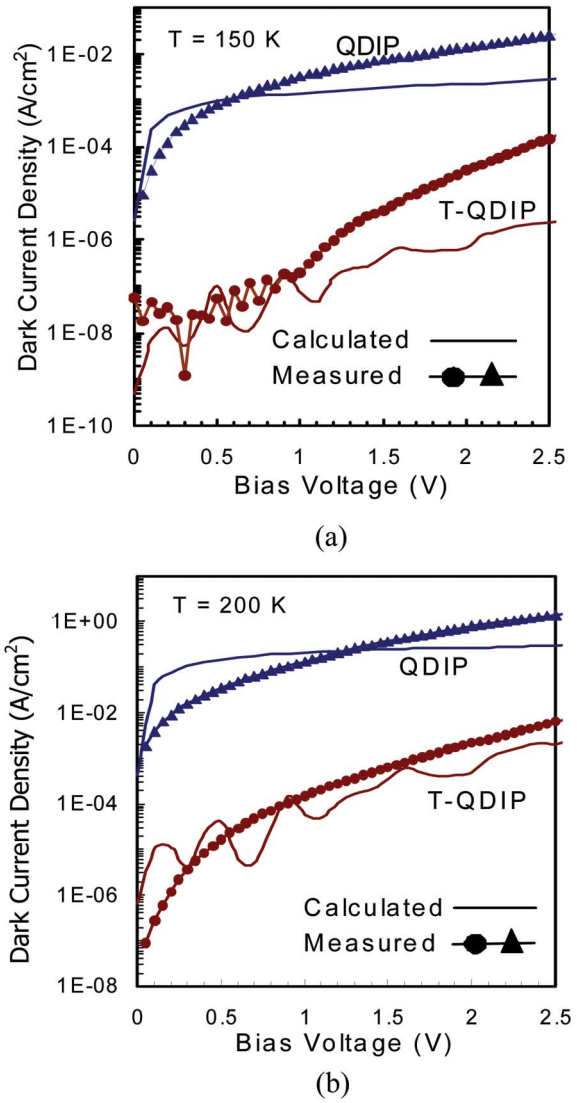

Fig. 3. *Comparison of calculated and measured dark current densities as a function of bias voltage for conventional and tunneling QDIPs using InAs/GaAs quantum dots at: (a) $T = 150$ K and (b) $T = 200$ K.*

details of growth and device fabrication are described in the next section. The measured dark current densities in the two devices are also plotted in Fig. 3, and agreement with the calculated data is reasonably good for both the conventional and tunneling designs. Disagreement at large bias values, particularly noticeable in Fig. 3(a), is due to the assumption that carrier equilibrium conditions exist, which is not true in the large bias range.

III. CHARACTERISTICS OF MIR AND FIR T-QDIPS

It is evident from the results presented in Section II that the double barrier tunneling heterostructure can greatly reduce the dark current in QDIPs. In the final design, a single $Al_{0.1}Ga_{0.9}As$ barrier is also included on the side of the dot opposite to the tunnel barriers. As shown in Fig. 4(a), the inclusion of this layer creates a quantum well and quasi-bound final states for the photoexcited electrons from the quantum dots. These states are designed to resonate with the tunnel states in the double barrier heterostructure. Furthermore, the energy position of the states in the well can be tuned by varying the distance of

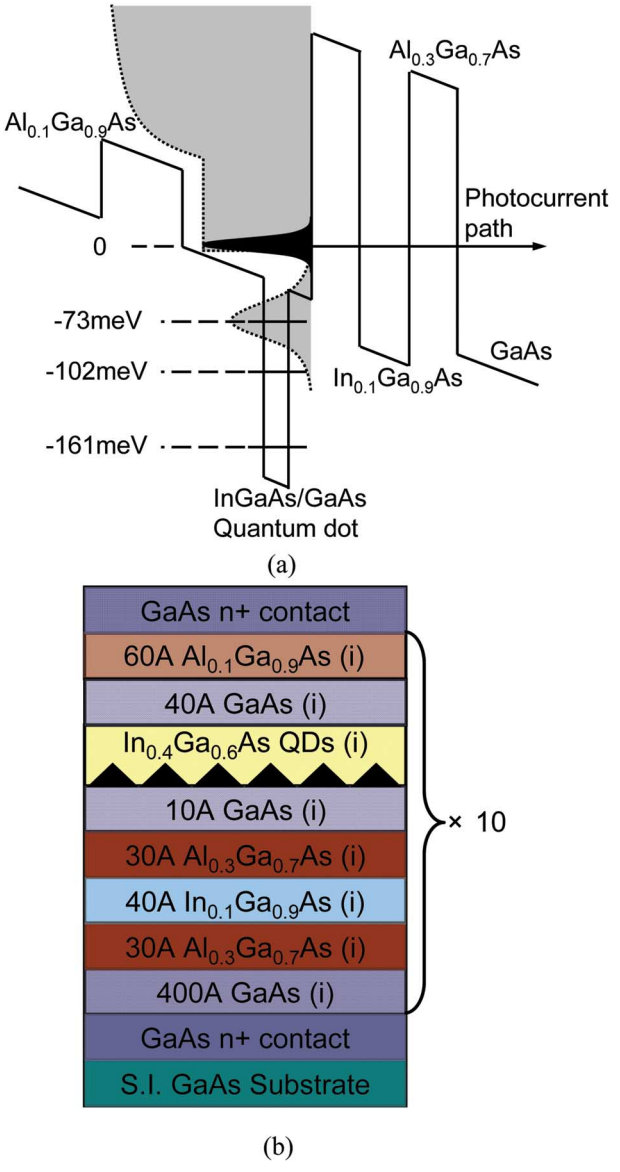

Fig. 4. *(a) Conduction band profile of one period in the absorption region of an InGaAs/GaAs T-QDIP with a GaAs/$Al_{0.3}Ga_{0.7}As$ resonant tunneling heterostructure with an injector well. (b) Corresponding device heterostructure grown by molecular beam epitaxy on (001) GaAs. All the other layers, except the Si-doped GaAs contact layers, are undoped.*

the $Al_{0.1}Ga_{0.9}As$ barrier from the quantum-dot layer, thereby providing tunability of the absorption peak wavelength.

The bound state energies in the quantum dots, also indicated in Fig. 4(a), were calculated by an eight-band $\mathbf{k}\cdot\mathbf{p}$ model, wherein the strain distribution in the dots were obtained from a valence force field formulation. The energy levels in the quantum well, taking into account the presence of the two-dimensional wetting layer that precedes the three-dimensional island in every dot layer, is calculated by solving the one-dimensional Schrödinger equation. The calculated value of the absorption coefficient in an $In_{0.4}Ga_{0.6}As$ quantum dot is $\sim 10^4$ cm^{-1} for normal incidence. While this value is quite large, it should be noted that the absorbing region of a quantum-dot layer is very thin ($\sim$100 Å). Therefore, multiple dot layers are required to absorb a significant fraction of the incoming IR light.

A. Epitaxial Growth and Device Fabrication

The tunneling QDIP heterostructures, shown schematically in Fig. 4(b), were grown by molecular beam epitaxy on (001)-oriented semi-insulating GaAs substrate. The GaAs and $Al_{0.3}Ga_{0.7}As$ layers were grown at 610 °C and the undoped quantum dots were grown at 500 °C. Before initiating the growth of the quantum dots, 10 Å of GaAs was grown on the $Al_{0.3}Ga_{0.7}As$ barrier of the resonant tunneling heterostructure, to smoothen the growing surface. This was followed by the deposition of six monolayers of InGaAs to form the self-organized quantum dots. An $Al_{0.1}Ga_{0.9}As$ barrier of thickness 40 Å is incorporated on the other side of the dot, opposite to the double barrier. As shown in Fig. 4(b), ten dot layers with accompanying double barrier structures are grown, separated by 400 Å GaAs barrier layers. Growth is terminated with a 0.2 μm silicon-doped ($n = 2 \times 10^{18}$ cm^{-3}) GaAs top contact layer.

A standard, three-step photolithography, wet-etching, and contact metallization process was employed to fabricate the vertical n-i-n mesa-shaped QDIPs. The first step is the deposition of Ni/Ge/Au/Ti/Au by electron beam evaporation to form the top ring contact, defined by photolithography and lift-off techniques. Next, wet etching is done, with the top contact as the mask, to define the mesa-shaped active region for a single pixel. The same multilayered metal evaporation is next done to define the bottom ring contact. The active area of the detector exposed to IR radiation is determined by the inner radius of the top ring contact (200 μm) and is approximately 1.26×10^5 μm^2.

B. Results and Discussion

Measurement Techniques: The devices are mounted on chip carriers with silver epoxy and individual devices are wire bonded to separate leads of the carriers. These are then mounted in a variable temperature liquid He cryostat. The dark current–voltage (I–V) characteristics are measured with a Hewlett-Packard 4145 semiconductor parameter analyzer. Measurements are made for both bias polarities, where a positive bias denotes a positive polarity of the top contact. The band diagram shown in Fig. 4(a) is for a negative applied bias.

The spectral response and calibrated responsivity spectra of the devices are measured, under normal incidence, with a GLOBAL broadband source. The spectral response of the device under test and a composite bolometer, with a known sensitivity, are measured with a S2000 Fourier transform infrared spectrometer (FTIR). The two spectra are obtained concurrently with the same combination of optical window, beamsplitter and filters, so that the optical path is identical.

The specific detectivity (D^*) of the devices at different temperatures and applied biases is obtained from the measured peak responsivity R_p and noise density spectra, S_i. The latter are measured with a dual channel fast Fourier Transform (FFT) signal analyzer and a low noise preamplifier. A thick copper plate is used as the radiation block to provide the dark conditions for the measurements.

Dark Current and Spectral Response: Measured bias-dependent dark current densities in the temperature range of 80 K–300 K are shown in Fig. 5. The fact that the minimum dark current is not at 0 V at 80 K is due to instrumental error. Compared to Fig. 3(a), the measured dark current density in Fig. 5 is higher. The main reason for this difference is the difference in thickness of the $Al_{0.3}Ga_{0.7}As$ barrier layers. A slight asymmetry observed for opposite bias polarities in the low-temperature data arises from the asymmetry in the dot heterostructure. From the data of Fig. 5, the values of J_{dark} at a bias of 1 V

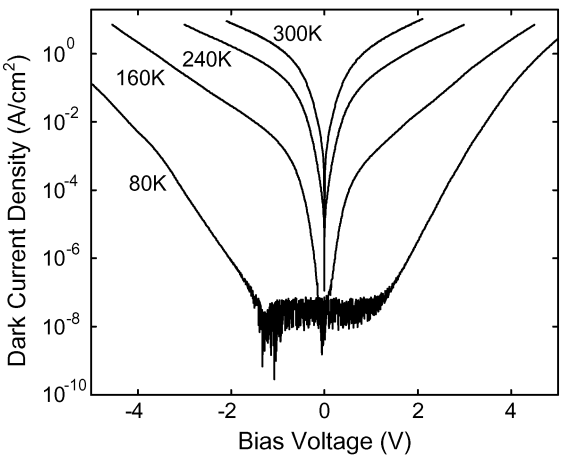

Fig. 5. *Measured dark current density of tunnel QDIP as a function of bias in the temperature range of 80 K–300 K.*

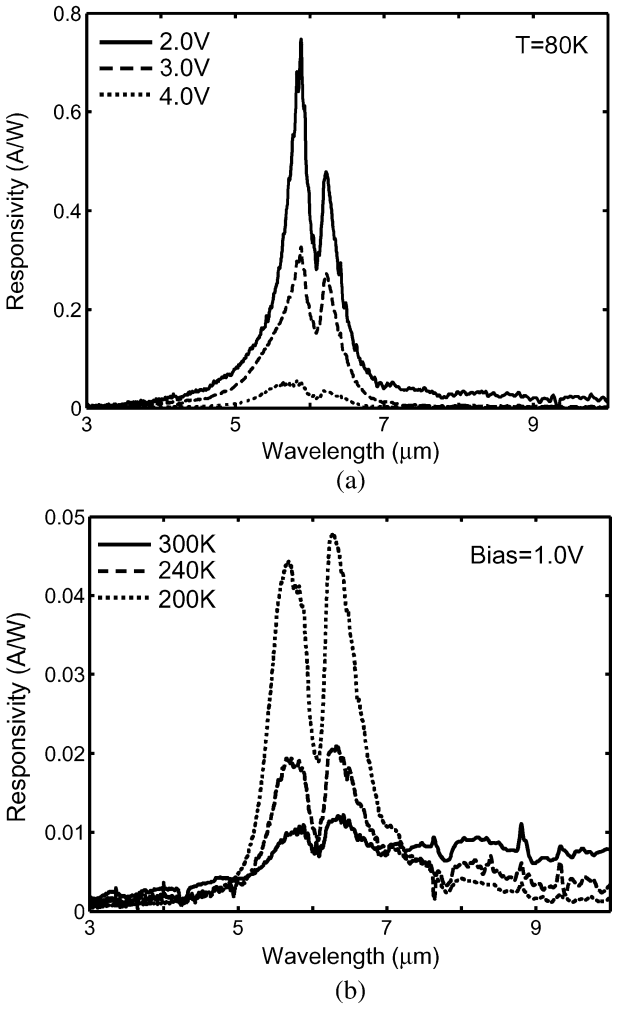

Fig. 6. *Measured spectral responsivity of tunnel QDIP in MIR range: (a) in the bias range 2–4 V at 80 K and (b) in the temperature range 240 K–300 K, under 1 V bias.*

are 1.61×10^{-8}, 1.01×10^{-3}, and 1.55 A/cm^2 at 80 K, 160 K, and 300 K, respectively. These values are very low for QDIPs.

Fig. 6(a) depicts the dominant midinfrared spectral response of the tunnel QDIP for different bias values measured at 80 K. Fig. 6(b) shows the same peaks measured at higher temperatures, up to 300 K. Compared to conventional QDIPs, with identical $In_{0.4}Ga_{0.6}As$ quantum dots exhibiting midinfrared peak response near 8 μm [19], the T-QDIP response has a blue shift. The reason is that the AlGaAs barriers surrounding the dots raise the final transition state to higher energies in the T-QDIP, compared to a conventional device with identical quantum dots. It is apparent that the response centered at 6 μm consists of two closely spaced peaks at 5.7 and 6.2 μm. The transition wavelength of 6 μm is in excellent agreement with the designed and calculated transition energy of 161 meV for the photoexcited electrons from the ground state in the quantum dot to the quasi-bound state in the well. The peaks at 5.7 and 6.2 μm arise from overlap of the wavefunctions of the quantum-well states and the bound states of the double barrier heterostructure. The twin peaks provide experimental evidence of resonant tunneling in the operation of the device. The estimated value of $\Delta\lambda/\lambda$ for the 5.7 μm peak is 6%. From the data of Fig. 6(a) and (b), the peak responsivity and quantum efficiency are, respectively, 0.75 A/W and 16% (4 V bias) at 80 K and 0.05 A/W and 1.1% (2 V bias) at 300 K.

While the 6 μm response is dominant for ambient temperatures below 200 K, long wavelength IR (LWIR) response at 11 and 17 μm are observed in the T-QDIPs at higher temperatures. It is worthwhile to note that the long wavelength (17 μm) absorption becomes significant at temperatures higher than 200 K and, as is evident from Fig. 7, its peak responsivity, $\sim$0.16 A/W, at 300 K is even higher than that of the 6 μm peak. With reference to the calculated energies of the bound and quasi-bound states in the dot and well, shown in Fig. 4, it is apparent that the absorption peak at $\sim$6 μm results from transition of photoexcited electrons from the dot ground state to the quasi-bound state in the well ($\Delta E = 161$ meV). The broad peak centered at 17 μm results from transitions from the second excited state of the dot to the well state ($\Delta E = 73$ meV). The width of the peak is due to the transition being in the LWIR region. In fact, the transition linewidth is only $\sim$26 meV, which is remarkably close to the inhomogenenous broadening of the QD states at 300 K. We believe that the 17 μm transition is dominant at high temperatures because the probability of occupation of the dot excited states increases with temperature. Due to the symmetry of the dot geometry, the excited states have a

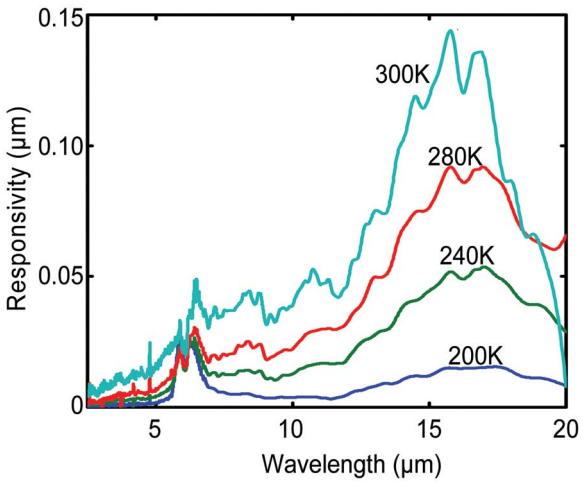

Fig. 7. *Measured spectral responsivity in the long wavelength range of tunnel QDIP in the temperature range 240–300 K.*

higher degeneracy than the ground state. The degeneracy of the second excited states is eight, while it is two for the ground state. Therefore, the total number of carriers in the excited states can be comparable to, or larger than, that in the ground state at high temperatures although the occupation probability is lower. Additionally, for the same incident power, there are more photons at 17 μm than at 6 μm. These characteristics help to explain a higher absorption peak at 17 μm compared to that at 6 μm for temperatures of 280 K and 300 K. It may be noted that the weak transition at $\sim$11 μm corresponds almost exactly to the energy separation between the first excited dot state and the well state ($\Delta E = 102$ meV). The selection rules may account for the weak transition. The wavefunction of the first excited dot states is anti-symmetrical in space and the wavefunction of the final states in the well is almost symmetrical near the dot layer. These give rise to a small transition momentum matrix as well as low responsivity. In contrast, all initial and final states corresponding to the 6 and 17 μm transitions are symmetrical and the transitions are allowed. Finally, it is extremely important to note that it is the low dark current in the T-QDIP that makes detection possible at these high temperatures.

Specific Detectivity: The measured values of D^* for the 6 μm peak at $T = 80$ K are plotted in Fig. 8(a) as a function of bias. The value of D^* reaches a maximum value of 2.4×10^{10} cm $\cdot$ Hz$^{1/2}$/W at 2 V and decreases again due to the monotonic increase of the dark current with bias. This value is amongst the highest measured for QDIPs at 80 K. The values of D^* for the 17 μm response at a bias of 1 V are plotted in Fig. 8(b) as a function of temperature. The values of D^* are in the 10^7 cm $\cdot$ Hz$^{1/2}$/W range.

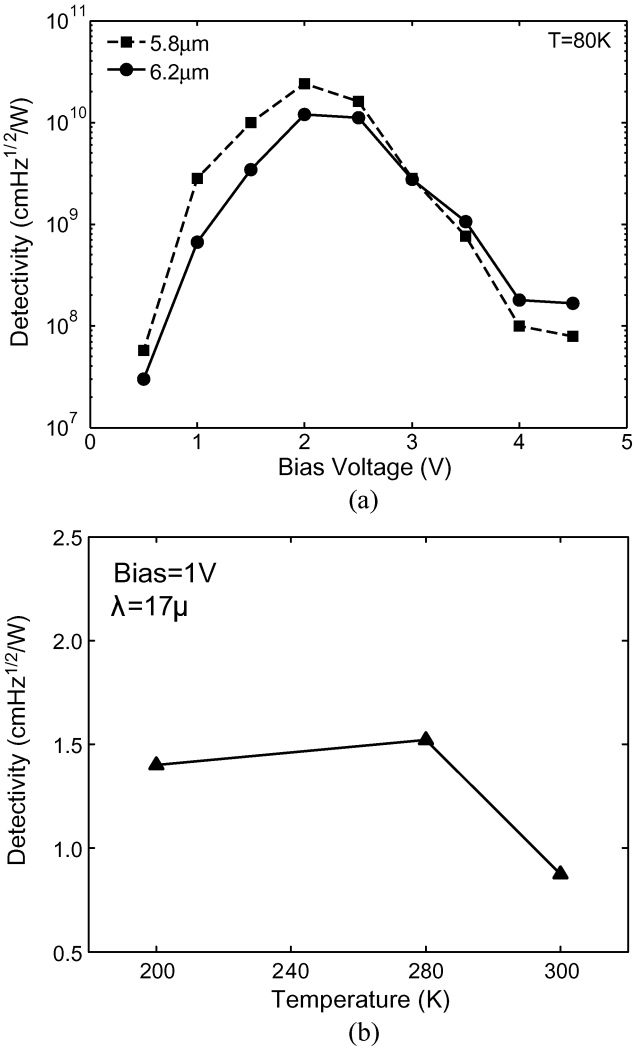

Fig. 8. *(a) Peak detectivity of tunnel QDIP as a function of bias for the 5.7 and 6.2 μm response at 80 K. (b) Peak detectivity as a function of temperature for the 17 μm response derived from noise spectra measurements.*

IV. TUNNEL QDIPs FOR TERAHERTZ DETECTION

For detection of terahertz radiation, the energy spacing between the confined state in the dot and the quasi-bound states in the well has to be of the order of 10 meV or less. To achieve this, we have grown $In_{0.6}Al_{0.4}As/GaAs$ quantum dots in the active region of the devices, instead of the more conventional InAs dots. Incorporation of Al into the dot material serves two purposes: first, due to the larger bandgap of InAlAs, compared to InAs, the bound state energies are closer to the GaAs barrier energy, and hence to the quasi-bound states in the well. Second, due to the smaller migration rate of Al adatoms on the growing surface during epitaxy, the Al-containing islands (dots) are smaller in size compared to InAs dots and the dot confined states are higher in energy. In this study, the dot size in the devices was also varied, by varying the MBE growth parameters, to tune the absorption frequency. Finally, the density of $In_{0.6}Al_{0.4}As$ dots ($\sim 3 \times 10^{11}$ cm^{-2}) is generally an order of magnitude larger than that of InAs dots, which helps to absorb more of the incident radiation. In this section, we describe the performance characteristics of tunnel QDIPs, incorporating $In_{0.6}Al_{0.4}As/GaAs$ self-organized quantum dots of reduced size in the active region, which exhibit spectral response with peak and cut-off wavelength of 50 μm and 75 μm ($\sim$4.0 THz), respectively.

The average size of the $In_{0.6}Al_{0.4}As$ dots was estimated from atomic force microscopy (AFM) measurements. An AFM image of an ensemble of the smaller sized dots is also shown in Fig. 9(a). The base and height of the near-pyramidal dots are $\sim$140 Å and $\sim$45 Å, respectively. As described in Section III, the 8-band $\mathbf{k} \cdot \mathbf{p}$ model is also used to calculate the electronic states in these quantum dots. The quasi-bound final states in the well are also calculated and the energy difference between the dot-to-well transition is 24.6 meV, which is in the THz range.

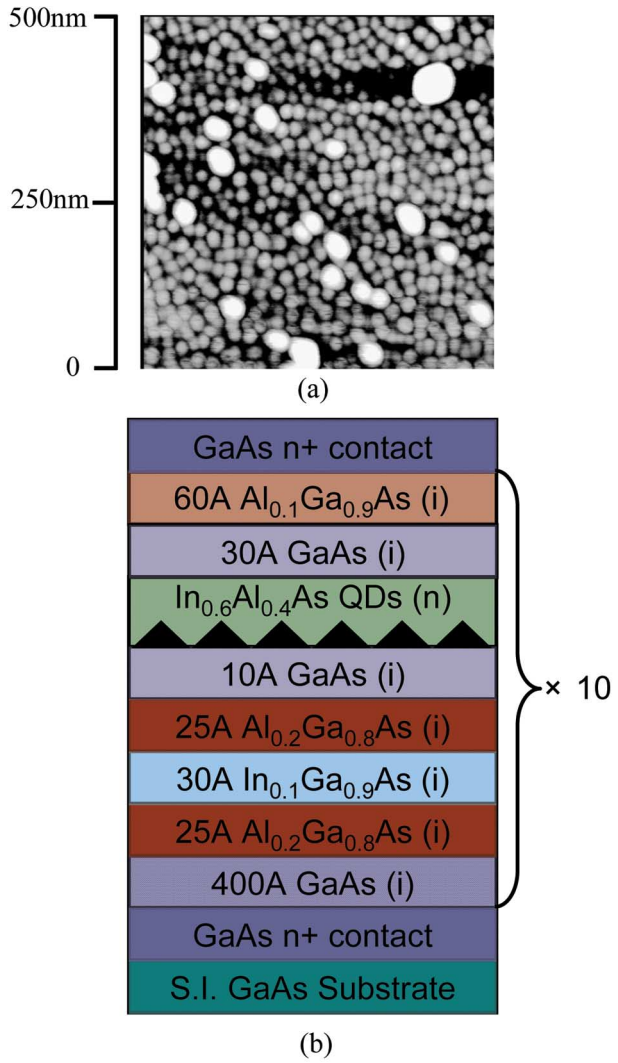

Fig. 9. *Atomic force microscopy image of $In_{0.6}Al_{0.4}As$/GaAs dots. (b) Schematic heterostructure of terahertz T-QDIP grown by molecular beam epitaxy.*

The complete device heterostructure, grown on (001)-oriented semi-insulating GaAs substrate, is schematically shown in Fig. 9(b). The fabricated device is inserted into a liquid helium dewar equipped with special windows which are transparent to very long wavelength light (10–80 μm). The dark current density of the device, with the smaller sized InAlAs dots, as a function of bias voltage and temperature, is shown in Fig. 10. The dark current densities at a bias of 1 V are 4.77×10^{-8}, 2.03×10^{-2}, and 4.09 A/cm^2 at 4.2 K, 80 K, and 150 K respectively. These values are very low compared to other THz detectors [20], [21]. We believe this is due to the presence of the double barrier tunnel heterostructure. For comparison, the dark current densities in a device with larger sized dots, measured at 80 K, are also included. It is apparent that devices with larger dots are more suitable for high temperature operation.

The calibrated spectral response of the T-QDIP with smaller dots at 4.6 K, with bias of 1.0 V, is shown Fig. 11(a). The peak responsivity is about 0.45 A/W and the wavelength corresponding to this peak is around 50 μm, which agrees with the calculated energy difference between the QD bound state and the quasi-bound state in the well of 24.6 meV (50.4 μm). The cutoff wavelength is $\sim$75 μm, which corresponds to $\sim$4.0 THz. The transition between the dot state and the state in the well is expected to be sensitive to normal incidence or s-polarized radiation. This has been verified earlier in QDIPs. In the dot-well system, the states in the well are no-longer z-confined, but also have a radial component. The dark region (dip) in the spectral response centered at $\sim$36 μm is due to longitudinal optical phonon absorption in GaAs, which has been observed for other GaAs based detectors [20], [21]. The spectral response appears to be fairly broad. The transition is believed to be from the dot bound states to quasi-bound states in the well and the spectral width of such transition will not match the observed full-width at half-maximum (FWHM) $\sim$35 μm, which corresponds to 23 meV. We attribute the observed linewidth to size nonuniformity of the self-organized dots which give rise to linewidth $\sim$30–40 meV in the interband photoluminescence spectra. Fig. 11(b) shows responsivity spectra at 150 K from a device with the larger sized $In_{0.6}Al_{0.4}As$ dots. The long-wavelength response is shifted to shorter wavelengths. The device can be operated at a temperature of 150 K, which is high compared to other photon-based THz detectors. In order to achieve 1–3 THz operation at reasonably high temperature, the dot size needs to be reduced, the size uniformity improved, and the tunnel heterostructure further optimized to keep the dark current low. The dot size can be reduced by increasing the Al content in the dots and by reducing the growth

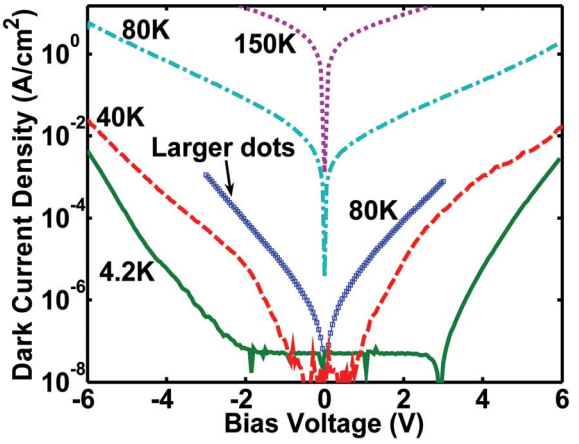

Fig. 10. *Measured dark current density of terahertz T-QDIP as a function of bias and temperature.*

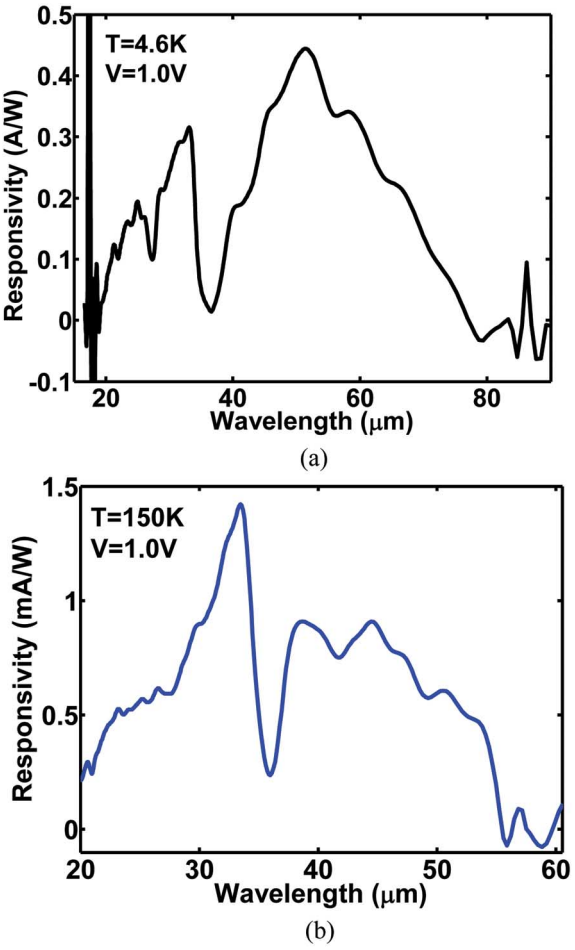

Fig. 11. ***Measured spectral responsivity of terahertz T-QDIP at: (a) 4.2 K and (b) 150 K under bias of 1 V.***

temperature. The measured D^* values are 1.64×10^8 and 4.98×10^7 cm $\cdot$ Hz$^{1/2}$/W at 4.6 K and 80 K, respectively, under a bias of 1 V.

Before concluding, it is worthwhile to make some comments regarding the challenges involved in the design and fabrication of tunnel QDIPs. The devices, as we have designed them, incorporated $In_{0.1}Ga_{0.9}As$ layers in addition to the quantum dots, which are both lattice mismatched to GaAs. Due to the accumulative strain of successive periods of the tunnel structure in the active region, a limit is placed on the number of periods that can be grown without generating dislocations. We found ten dot layers (periods) to be optimal, which results in the quantum efficiency of the T-QDIP being lower than a QDIP with a larger number of dot layers. As a result, the responsivity and detectivity suffer. Choice of the other heterostructure systems may alleviate this problem to some extent. It may also be noted that while the tunnel QDIP design enables a reduction in dark current, a reduction in the photocurrent also takes place due to the size distribution of self-organized quantum dots. This may also lower the responsivity of a T-QDIP, compared to a conventional device. However, this degradation may be compensated, to a large extent, by the fact that the photoexcited carriers in the T-QDIP undergo transitions from a dot bound state to a quasi-bound state formed in the quantum well.

V. CONCLUSION

In conclusion, the tunnel QDIP is a versatile device in which the incorporation of a double barrier resonant tunneling heterostructure with each quantum-dot layer helps to significantly lower the dark current and enable high temperature operation. The quantum-dot heterostructure can be engineered for the detection of photons in the MIR, FIR, and THz frequencies. We demonstrate dark currents as low as 0.1 A/cm^2 at room temperature and operation at temperature in the range 80 K–300 K at all frequency ranges with acceptable values of D^* and responsivity. With source improvement in device design, tunnel QDIPs will be externally desirable for high temperature detection and imaging at all frequencies. ■

REFERENCES

[1] J. Phillips, K. Kamath, and P. Bhattacharya, "Far-infrared photoconductivity in self-organized InAs quantum dots," *Appl. Phys. Lett.*, vol. 72, pp. 2020–2021, 1998.

[2] D. Pan, E. Towe, and S. Kennerly, "Normal incidence intersubband (In,Ga)As/GaAs quantum dot infrared photodetectors," *Appl. Phys. Lett.*, vol. 73, pp. 1937–1939, 1998.

[3] S. Maimon, E. Finkman, G. Bahir, S. E. Schacham, J. M. Garcia, and P. M. Petroff, "Intersublevel transitions in InAs/GaAs quantum dot photodetectors," *Appl. Phys. Lett.*, vol. 73, pp. 2003–2005, 1998.

[4] B. Kochman, A. D. Stiff-Roberts, S. Chakrabarti, J. D. Phillips, S. Krishna, J. Singh, and P. Bhattacharya, "Absorption, carrier lifetime, and gain in InAs-GaAs quantum-dot infrared photodetectors," *IEEE J. Quantum Electron.*, vol. 39, no. 3, pp. 459–467, Mar. 2003.

[5] J. Urayama, T. B. Norris, J. Singh, and P. Bhattacharya, "Observation of phonon bottleneck in quantum dot electronic relaxation," *Phys. Rev. Lett.*, vol. 86, p. 4930, 2001.

[6] J. Phillips, P. Bhattacharya, S. W. Kennerly, D. W. Beekman, and M. Dutta, "Self-assembled InAs-GaAs quantum-dot intersubband detectors," *IEEE J. Quantum Electron.*, vol. 35, no. 6, pp. 936–943, Jun. 1999.

[7] S. Krishna, S. Raghavan, G. von Winckel, A. Stintz, G. Ariyawansa, S. G. Matsik, and A. G. U. Perera, "Three-color ($\lambda_{p1} = 3.8$ μm, $\lambda_{p2} = 8.5$ μm, and $\lambda_{p3} = 23.2$ μm) InAs/InGaAs quantum-dots-in-a-well detector," *Appl. Phys. Lett.*, vol. 83, p. 2745, 2003.

[8] L. Jiang, S. S. Li, N. T. Yeh, J. I. Chie, C. E. Ross, and K. S. Jones, "$In_{0.6}Ga_{0.4}As$/GaAs quantum-dot infrared photodetector with operating temperature up to 260 K," *Appl. Phys. Lett.*, vol. 82, p. 1986, 2003.

[9] E. T. Kim, A. Madhukar, Z. Ye, and J. C. Campbell, "High detectivity InAs quantum dot infrared photodetector," *Appl. Phys. Lett.*, vol. 84, pp. 3277–3279, 2004.

[10] S. Chakrabarti, A. D. Stiff-Roberts, P. Bhattacharya, S. D. Gunapala, S. Bandara, S. B. Rafol, and S. W. Kennerly, "High temperature operation of InAs-GaAs quantum dot infrared photodetectors with large responsivity and detectivity," *IEEE Photon. Technol. Lett.*, vol. 16, no. 5, pp. 1361–1363, May 2004.

[11] S. Raghavan, P. Rotella, A. Stintz, B. Fuchs, S. Krishna, C. Morath, D. A. Cardimona, and S. W. Kennerly, "High-responsivity, normal-incidence long-wave infrared ($\lambda \sim 7.2$ μm) InAs/In0.15Ga0.85As dots-in-a-well detector," *Appl. Phys. Lett.*, vol. 81, pp. 1369–1372, 2002.

[12] S. Chakrabarti, A. D. Stiff-Roberts, P. Bhattacharya, and S. W. Kennerly, "High responsivity AlAs/InAs/GaAs superlattice quantum dot infrared detector," *Electron. Lett.*, vol. 40, pp. 197–198, 2004.

[13] X. H. Su, S. Chakrabarti, A. D. Stiff-Roberts, J. Singh, and P. Bhattacharya, "Novel quantum dot infrared photodetector design based on double-barrier resonant tunneling," *Electron. Lett.*, vol. 40, p. 1082, 2004.

[14] X. H. Su, S. Chakrabarti, P. Bhattacharya, G. Ariyawansa, and A. G. U. Perera, "A resonant tunneling quantum-dot infrared photodetector," *IEEE J. Quantum Electron.*, vol. 41, no. 7, pp. 974–979, Jul. 2005.

[15] P. Bhattacharya, X. H. Su, S. Chakrabarti, G. Ariyawansa, and A. G. U. Perera, "Characteristics of a tunneling quantum-dot infrared photodetector operating at room temperature," *Appl. Phys. Lett.*, vol. 86, p. 191 106, 2005.

[16] X. H. Su, J. Yang, P. Bhattacharya, G. Ariyawansa, and A. G. U. Perera, "Terahertz detection with tunneling quantum dot intersublevel photodetector," *Appl. Phys. Lett.*, vol. 89, p. 031117, 2006.

[17] H. Jiang and J. Singh, "Strain distribution and electronic spectra of InAs/GaAs self-assembled dots: An eight-band study," *Phys. Rev. B.*, vol. 56, pp. 4696–4701, 1997.

[18] B. Kochmann, A. D. Stiff-Roberts, S. Chakrabarti, J. D. Phillips, S. Krishna, J. Singh, and P. Bhattacharya, "Absorption, carrier lifetime and gain in InAs/GaAs quantum dot infrared photodetectors," *IEEE J. Quantum Electron.*, vol. 39, no. 3, pp. 459–467, Mar. 2003.

[19] P. Bhattacharya, X. H. Su, and J. Singh. (2006, Oct.). Resonant tunneling quantum dot infrared photodetector: High temperature detection at infrared and terahertz frequencies. *IEEE LEOS Newsletter*. [Online]. *20(5)*, pp. 13–18. Available: http://www.ieee.org/organizations/pubs/newsletters/leos/oct06/pg13_18.pdf

[20] M. B. M. Rinzan, A. G. U. Perera, S. G. Matsik, H. C. Liu, Z. Wasilewski, and M. Buchanan, "AlGaAs emitter GaAs barrier terahertz detector with a 2.3 THz threshold," *Appl. Phys. Lett.*, vol. 86, p. 071112, 2005.

[21] D. G. Esaev, M. B. M. Rinzan, S. G. Matsik, A. G. U. Perera, H. C. Liu, B. N. Zvonkov, V. I. Gavrilenko, and A. A. Belyanin, "High performance single emitter homojunction interfacial work function far infrared detectors," *J. Appl. Phys.*, vol. 95, p. 512, 2004.

ABOUT THE AUTHORS

Pallab Bhattacharya (Fellow, IEEE) received the M.Eng. and Ph.D. degrees from the University of Sheffield, Sheffield, U.K., in 1976 and 1978, respectively.

From 1978 to 1983, he was on the faculty of Oregon State University, Corvallis, and since 1984 he has been with the University of Michigan, Ann Arbor. He was also an Invited Professor at the Ecole Polytechnic Federale de Lausanne, Switzerland, from 1981 to 1982. He is currently the Charles M. Vest Distinguished University Professor of Electrical Engineering and Computer Science and the James R. Mellor Professor of Engineering in the Department of Electrical Engineering and Computer Science at the University of Michigan. He was an Editor of the IEEE TRANSACTIONS ON ELECTRON DEVICES and is Editor-in-Chief of *Journal of Physics D*. He has edited *Properties of Lattice-Matched and Strained InGaAs* (U.K.: INSPEC, 1993) and *Properties of III-V Quantum Wells and Superlattices* (U.K.: INSPEC, 1996). He has also authored the textbook *Semiconductor Optoelectronic Devices* (Prentice Hall, 2nd ed.). His teaching and research interests are in the areas of compound semiconductors, low-dimensional quantum confined systems, nanophotonics, and optoelectronic integrated circuits. He is currently working on high-speed quantum-dot lasers, quantum-dot infrared photodetectors, photonic crystal quantum-dot devices, and spin-based heterostructure devices.

Prof. Bhattacharya has received the John Simon Guggenheim Fellowship, the IEEE (EDS) Paul Rappaport Award, the IEEE (LEOS) Engineering Achievement Award, the Optical Society of America (OSA) Nick Holonyak Award, the SPIE Technical Achievement Award, the Quantum Devices Award of the International Symposium on Compound Semiconductors, and the IEEE (Nanotechnology Council) Nanotechnology Pioneer Award, and has been selected to receive the 2008 TMS John Bardeen Award. He has also received the S. S. Attwood Award, the Kennedy Family Research Excellence Award, and the Distinguished Faculty Achievement Award from the University of Michigan. He is a Fellow of the American Physical Society, the Institute of Physics (U.K.), and the Optical Society of America.

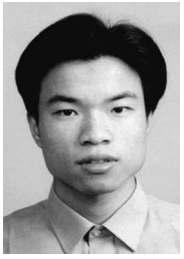

Xiaohua Su received the B.S. degree in material science from University of Science and Technology of China, Hefei, in 2000, the M.S. degrees in physics and electrical engineering from the Georgia Institute of Technology, Atlanta, in 2002 and 2003, respectively, and the Ph.D. degree in electrical engineering form University of Michigan, Ann Arbor, in 2006.

He is currently an Integrated Circuit Design Engineer at Linear Technology Corporation, Colorado Springs, CO, where he is working on high-performance analog chips for power management.

G. Ariyawansa, photograph and biography not available at the time of publication.

A. G. U. Perera, photograph and biography not available at the time of publication.